

Multiple Liquid Crystalline Geometries of Highly Compacted Nucleic Acid in a dsRNA Virus

Serban L. Ilca¹, Xiaoyu Sun², Kamel El Omari³, Abhay Kotecha^{1,4}, Felix de Haas⁴, Frank diMaio⁵, Jonathan M. Grimes^{1,3}, David I. Stuart^{1,3}, Minna M. Poranen², Juha T. Huiskonen^{1,6}

¹ Division of Structural Biology, Wellcome Centre for Human Genetics, University of Oxford, Roosevelt Drive, OX3 7BN, Oxford, United Kingdom

² Molecular and Integrative Biosciences Research Programme, Faculty of Biological and Environmental Sciences, University of Helsinki, Viikinkaari 9, 00014 Helsinki, Finland

³ Diamond Light Source Ltd., Diamond House, Harwell Science and Innovation Campus, Didcot, Oxfordshire, OX11 0DE, United Kingdom

⁴ Thermo Fisher Scientific, Achtseweg Noord 5, 5651 GG Eindhoven, The Netherlands

⁵ Molecular Engineering and Sciences, University of Washington, Box 351655, Seattle, WA 98195, USA

⁶ Helsinki Institute of Life Science HiLIFE and Molecular and Integrative Biosciences Research Programme, Faculty of Biological and Environmental Sciences, University of Helsinki, Viikinkaari 1, 00014 Helsinki, Finland

Summary

Characterising the genome of mature virions is pivotal to understanding the highly dynamic processes of virus assembly and infection. In dsDNA and dsRNA viruses, the packaged double-stranded nucleic acid, constrained by the rigidity of the double-helix, adopts a liquid crystalline arrangement^{1–5}. Owing to the different cellular fates of DNA and RNA, the life cycles of these viruses are strikingly dissimilar. Current models suggest that dsDNA viruses predominantly display single-spoiled conformations due to the lack of genome segmentation and the absence of intra-capsid transcriptional machinery^{6–8}. As dsRNA triggers host defence mechanisms if released into the cytoplasm⁹, dsRNA viruses retain their genomes within a core particle containing the enzymes required for RNA replication and transcription^{10,11,12}. Their genomes vary greatly in the degree of segmentation. In reoviruses (*Reoviridae*, 10–12 segments) the genome organizes in nonspoiled fashion and is tightly associated with the viral RNA-dependent RNA polymerases (RdRPs)^{11–14}. However, whether this organization is generally applicable in dsRNA viruses remains unknown. Here, we use cryogenic electron microscopy (cryo-EM) to show that dsRNA viruses

can adopt dsDNA-like single-spoiled genome organisations by resolving the dsRNA genome structure of bacteriophage $\phi 6$ (*Cystoviridae*, 3 segments). We find that in this group of viruses, the RdRPs do not direct the genome arrangement and that the dsRNA can adopt multiple organizations. We build a model for 90% of the genome allowing us to quantify variation in the packing density and to describe the different liquid crystalline geometries exhibited by the tightly compacted nucleic acid. The results enable us to extend the canonical model for dsDNA packing to a model organism for the study of packaging and intra-capsid transcription in dsRNA viruses.

Main text

Bacteriophage $\phi 6$ of the *Cystoviridae* family is a model for the study of genome packaging, replication, and transcription in dsRNA viruses. The $\phi 6$ nucleocapsid encompasses ~8–12 copies of the RdRP (P2) and a tri-segmented genome^{15–18}. To elucidate the dsRNA genome organisation in $\phi 6$, we first determined the structure of the icosahedral double-shelled capsid to 3.5 Å resolution by cryo-EM (**Fig 1a; Extended Data Figure 1; Extended Data Tables 1, 2**). Consistent with our earlier findings, 240 trimers of the P8 and 60 asymmetric P1_A–P1_B dimers create the outer and inner capsid shells, respectively¹⁸. Employing a multimodal priors maximum likelihood refinement and volume classification without any symmetry constraints (see **Methods**), we resolved several asymmetric structures of the dsRNA below radius of ~220 Å (**Fig 1b, Extended Data Figure 1, Extended Data Table 2**). In some regions, the major and minor grooves of the A-form double helix are discernible (**Fig 1b**, inset). Most of the dsRNA follows an approximate D3 symmetry (**Fig 1c**) with five layers of supercoiled dsRNA spooled around an icosahedral three-fold symmetry axis (**Fig 1d; Extended Data Figure 2**). In each layer, the central equatorial parts of the spool are considerably better resolved than the top and bottom. In most areas, however, individual strands of dsRNA are resolved (**Extended Data Figure 2**).

The first (outer) layer displayed several slightly different pseudo D3 geometries ($pD3$, $pD3'$, $pD3'-1$, $pD3'-2$, $pD3'-3$; **Extended Data Figure 1**; see also **Fig 3**). The first layer was particularly well resolved in $pD3'-1$. This map, together with the $pD3$ map where the resolved parts of the dsRNA strands in layers 2–5 were unambiguous, was used to build a model for ~90% of dsRNA genome (total length 13,385 bp; **Fig 1e,f; Extended Data Figure 2**). Layers 1–4 are centered at 201, 170, 141, and 107 Å radius, respectively, and the fifth layer resides between radii 65–100 Å (**Fig 1d**). The mean inter-strand distance is 26 Å between strands in the same layer and 29 Å between strands in different layers. The first four layers 1–4 are organized as nearly co-axial right-handed spools with the inclination of the double helix axes to the spool axis being 82, 77, 77 and 81°, respectively (**Fig 1f**). The innermost RNA does not follow this spooled arrangement. Instead, it is a barrel-like assembly of twelve ordered stretches of dsRNA, wound in a left-handed manner and running considerably more diagonally (36° inclination) than layers 1–4 at a distance of 70 Å from the spool axis (**Fig 1e,f**). This unique arrangement is likely required to avoid high degrees of curvature in the center of the capsid. The remaining ~10% of the RNA density, mainly at the spool ends, is disordered and could not be modeled. Notably, the RdRPs that are located under the 3-fold axes in unpackaged $\phi 6$ particles^{19,20} are displaced from these positions in the nucleocapsid and it is thus possible that they partially detach from the P1 shell as the capsid expands during

genome packaging and replication. The volume close to the spool axis, including the top and bottom parts of the spool, is the only significant volume not assigned to RNA. Thus the RdRPs might locate within this volume, a notion that requires verification by orthogonal methods²¹.

The model of the $\phi 6$ genome facilitated a detailed analysis how dsRNA packs in the confines of a viral capsid (**Fig 2**). The mean density was 350 mg/ml, consistent with our earlier findings²² and with density measurements for purified short dsDNA segments in the cholesteric phase^{23–26}. Densities for layers 1–5 were 389 ± 61 , 391 ± 40 , 355 ± 46 , 338 ± 38 and 278 ± 58 mg/ml, respectively, suggesting that layers 1 and 2 are more tightly packed than the rest (**Fig 2a**). The local packing of the strands is tighter at the spool equator than at the top and bottom of the spool (**Fig 2b,c**). To characterise the local packing geometries, we measured for each genome position how uniformly its neighboring strands are packed around it (defined by the polygonality index [PI], see **Methods**). PI varied over a wide range (~ 0.45 – 0.95 ; **Fig 2d**) in all layers suggesting different types of local packing geometries. A high order of polygonality can arise from either hexagonal or cubic arrangement of strands (**Fig 2e,f**). While the first layer has nearly equal amounts of these two types of arrangements (**Fig 2e**; **Extended Data Figure 3**), the fraction of cubic packing increases progressively in layers 2–5 (**Extended Data Figure 3**). The resolved ends of the spool follow neither of the two packing types, possibly due to higher curvature of RNA in these areas (**Fig 2e,f**). The angle of curvature increased progressively in layers 1–4, being 17 ± 6 , 18 ± 5 , 22 ± 6 , and 24 ± 4 degrees, respectively (**Fig 2g** and **2h**, inset). The spool ends that are less densely packed (**Fig 2c**) and less ordered than the middle of the spool (**Fig 2e,f**) are also highly curved (**Fig 2h,i**). Taken together, these analyses show that the genome is a cholesteric liquid crystal with local cubic and hexagonal geometries that are perturbed by the curvature of dsRNA.

The observed liquid crystalline packing prompted further analysis of different genome organizations by three-dimensional classification. This revealed a second, clearly distinct organization for layer 1 (**Fig 3a,b**; **Extended Data Figure 1**). Unlike the pseudo D3 symmetries discussed above (**Fig 1b**; **Fig 3a,c,e**) this organization shows an approximate two fold-symmetry ($pC2$; **Fig 3b,d**). This range of organisations is consistent with coarse grained molecular mechanics simulations of dsDNA which have suggested that double-stranded nucleic acid is unlikely to adopt a unique organisation⁸. Reconstructions of the $pD3$ sub-conformations ($pD3'$ -1, $pD3'$ -2, $pD3'$ -3) revealed differences in the positions where the RNA strands transition from the first layer to the second, providing an explanation for the multitude of discrete genome organizations in the first layer (**Fig 3f**). Furthermore, it is possible that other sub-conformations exist not detected in our analysis.

We hypothesized that the P1 shell partially orders the dsRNA, resulting in observable discrete organizations in the first layer. To exhaustively define all putative RNA–P1 interactions and their frequencies over the 60 P1_A and P1_B chains, we calculated all pairwise distances. Overall, positively charged amino acid side chains are slightly more frequent than negatively charged ones in close proximity to dsRNA (**Fig 4**, **Extended Data Figure 4**). Three asparagines (N279, N406, N570), which can potentially interact with the minor groove of the dsRNA²⁷ (**Fig 4c-e**; **Extended Data Figs 5** and **6**), as well as a helix comprising residues 205–217 were also often close to RNA (**Fig 4a,b**). This helix has three hydrophobic residues (M209, A212,

A216) aligned on the same face, and two positively charged residues (K215 and K208) on the two other exposed faces. The helix makes different types of contact to the RNA, either placed on top or side orthogonally to the axis of one strand of dsRNA (**Fig 4d,f**) or wedged parallel between two strands (**Fig 4e**). We propose that this helix plays a role as a guide for the nascent dsRNA segments during replication, in some areas acting as a spacer between the P1 shell and the RNA and in other areas wedging between the strands guiding their direction.

The organisation of $\phi 6$ dsRNA genome is remarkably different from that of cypoviruses^{13,14}, despite the fact that genomes in both of these viruses have an approximate D3 symmetry. This may be due to the several differences in the transcription mechanisms between *Cystoviridae* and *Reoviridae*: i. semi-conservative²⁸ vs conservative transcription mechanisms²⁹, ii. multiple polymerases capable of transcribing the same segment simultaneously³⁰ vs one RdRP/segment^{11–14,31}, and iii. RdRPs capable of replicating and transcribing RNA in the absence of other viral proteins³² vs RdRPs active only in association with the the capsid shell proteins^{33,34}. The observed nearly co-axial spooled organisation of the first four layers in cholesteric liquid crystal form resembles instead the conformations suggested for many dsDNA viruses^{6,8,23,35}. Whereas in the case of cypoviruses, only one conformation of the dsRNA genome was described, $\phi 6$ genome adopts multiple clearly distinct conformations. A further striking difference is that unlike the ordered RdRPs of cypoviruses that are proximal to the viral capsid^{13,14}, $\phi 6$ RdRPs were not detected in the three-fold symmetry positions they occupy in empty, unpackaged viral particles^{19,20}, many of these positions being instead occupied by dsRNA. This suggests that the RdRPs detach from the P1 shell, a possible mechanism to prime the particles for transcription. The perpendicular arrangement of RNA strands in the middle of the spool allows relatively unstrained occupation of this low radius region and might be a way to optimise the packing in conjunction with the co-axial spooled arrangement that accounts for the rest of the layers at higher radii. This arrangement may also provide the required flexibility and space for RNA transcription mechanics and the exit of the transcripts. Further cryo-EM studies are expected to prove whether this organisation is utilized more widely in dsRNA viruses, how it is created during genome replication, and how it enables transcription of the genome segments.

Acknowledgements

We thank Riitta Tarkiainen for technical assistance and Diamond Light Source for access and support of the Cryo-EM facilities (EM14856) at the UK national electron bio-imaging centre (eBIC) funded by the Wellcome Trust, MRC and BBSRC. The authors acknowledge the use of the Instruct-HiLIFE Biocomplex unit (University of Helsinki and Instruct-FI) and Academy of Finland support (grant 1306833) for the unit. This work was supported by European Research Council under the European Union's Horizon 2020 research and innovation programme (649053 to J.T.H.), a Wellcome Trust administrative support grant (203141/Z/16/Z), a Wellcome Trust four-year PhD studentship (109135/Z/15/A to S.L.I.), Academy of Finland (grant 272507 to M.M.P.), and Sigrid Jusélius Foundation (to M.M.P.).

Author contributions

S.L.I. reconstructed the genome maps and built the genome models. X.S. prepared the virus sample. A.K. reconstructed the nucleocapsid map. F.dH. assisted with data collection. F.dM. provided custom tools and together with J.M.G. advice for genome building. J.M.G., D.I.S., M.P. and J.T.H. provided supervision. K.E.O. analysed RNA–protein contacts. J.T.H. and S.L.I. analysed the data, prepared the figures and wrote the manuscript. All authors commented on the manuscript.

Author information

The authors declare the following competing interests: F.dH and A.K. are both employees of Thermo Fisher Scientific. Correspondence should be addressed to J.T.H. (juha@strubi.ox.ac.uk).

References

1. Speir, J. A. & Johnson, J. E. Nucleic acid packaging in viruses. *Curr. Opin. Struct. Biol.* **22**, 65–71 (2012).
2. Black, L. W. DNA packaging in dsDNA bacteriophages. *Annu. Rev. Microbiol.* **43**, 267–292 (1989).
3. Booy, F. P. *et al.* Liquid-crystalline, phage-like packing of encapsidated DNA in herpes simplex virus. *Cell* **64**, 1007–1015 (1991).
4. Lepault, J., Dubochet, J., Baschong, W. & Kellenberger, E. Organization of double-stranded DNA in bacteriophages: a study by cryo-electron microscopy of vitrified samples. *EMBO J.* **6**, 1507–1512 (1987).
5. Smith, D. E. *et al.* The bacteriophage straight phi29 portal motor can package DNA against a large internal force. *Nature* **413**, 748–752 (2001).
6. Cerritelli, M. E. *et al.* Encapsidated conformation of bacteriophage T7 DNA. *Cell* **91**, 271–280 (1997).
7. Jiang, W. *et al.* Structure of epsilon15 bacteriophage reveals genome organization and DNA packaging/injection apparatus. *Nature* **439**, 612–616 (2006).
8. LaMarque, J. C., Le, T.-V. L. & Harvey, S. C. Packaging double-helical DNA into viral capsids. *Biopolymers* **73**, 348–355 (2004).
9. Roers, A., Hiller, B. & Hornung, V. Recognition of Endogenous Nucleic Acids by the Innate Immune System. *Immunity* **44**, 739–754 (2016).
10. Patton, J. T. & Spencer, E. Genome replication and packaging of segmented double-stranded RNA viruses. *Virology* **277**, 217–225 (2000).
11. Gouet, P. *et al.* The highly ordered double-stranded RNA genome of bluetongue virus revealed by crystallography. *Cell* **97**, 481–490 (1999).
12. Yazaki, K. & Miura, K. Relation of the structure of cytoplasmic polyhedrosis virus and the synthesis of its messenger RNA. *Virology* **105**, 467–479 (1980).
13. Liu, H. & Cheng, L. Cryo-EM shows the polymerase structures and a nonspooled genome within a dsRNA virus. *Science* **349**, 1347–1350 (2015).
14. Zhang, X. *et al.* In situ structures of the segmented genome and RNA polymerase complex inside a dsRNA virus. *Nature* **527**, 531–534 (2015).
15. Day, L. A. & Mindich, L. The molecular weight of bacteriophage phi 6 and its nucleocapsid. *Virology* **103**, 376–385 (1980).

16. Sen, A. *et al.* Initial location of the RNA-dependent RNA polymerase in the bacteriophage Phi6 procapsid determined by cryo-electron microscopy. *J. Biol. Chem.* **283**, 12227–12231 (2008).
17. Sun, X., Bamford, D. H. & Poranen, M. M. Probing, by self-assembly, the number of potential binding sites for minor protein subunits in the procapsid of double-stranded RNA bacteriophage $\Phi 6$. *J. Virol.* **86**, 12208–12216 (2012).
18. Sun, Z. *et al.* Double-stranded RNA virus outer shell assembly by bona fide domain-swapping. *Nat. Commun.* **8**, 14814 (2017).
19. Nemecek, D., Qiao, J., Mindich, L., Steven, A. C. & Heymann, J. B. Packaging accessory protein P7 and polymerase P2 have mutually occluding binding sites inside the bacteriophage 6 procapsid. *J. Virol.* **86**, 11616–11624 (2012).
20. Ilca, S. L. *et al.* Localized reconstruction of subunits from electron cryomicroscopy images of macromolecular complexes. *Nat. Commun.* **6**, 8843 (2015).
21. Ikonen, T., Kainov, D., Timmins, P., Serimaa, R. & Tuma, R. Locating the minor components of double-stranded RNA bacteriophage $\Phi 6$ by neutron scattering. *J. Appl. Crystallogr.* **36**, 525–529 (2003).
22. Huiskonen, J. T. *et al.* Structure of the bacteriophage phi6 nucleocapsid suggests a mechanism for sequential RNA packaging. *Structure* **14**, 1039–1048 (2006).
23. Earnshaw, W. C. & Harrison, S. C. DNA arrangement in isometric phage heads. *Nature* **268**, 598–602 (1977).
24. Strzelecka, T. E., Davidson, M. W. & Rill, R. L. Multiple liquid crystal phases of DNA at high concentrations. *Nature* **331**, 457–460 (1988).
25. Livolant, F. & Leforestier, A. Condensed phases of DNA: Structures and phase transitions. *Prog. Polym. Sci.* **21**, 1115–1164 (1996).
26. Rey, A. D. Liquid crystal models of biological materials and processes. *Soft Matter* **6**, 3402–3429 (2010).
27. Morávek, Z., Neidle, S. & Schneider, B. Protein and drug interactions in the minor groove of DNA. *Nucleic Acids Res.* **30**, 1182–1191 (2002).
28. Van Etten, J. L., Burbank, D. E., Cuppels, D. A., Lane, L. C. & Vidaver, A. K. Semiconservative synthesis of single-stranded RNA by bacteriophage phi 6 RNA polymerase. *J. Virol.* **33**, 769–773 (1980).
29. Skehel, J. J. & Joklik, W. K. Studies on the in vitro transcription of reovirus RNA catalyzed by reovirus cores. *Virology* **39**, 822–831 (1969).
30. Usala, S. J., Brownstein, B. H. & Haselkorn, R. Displacement of parental RNA strands during in vitro transcription by bacteriophage phi 6 nucleocapsids. *Cell* **19**, 855–862 (1980).
31. Ding, K., Nguyen, L. & Zhou, Z. H. structures of polymerase complex and RNA genome show how aquareovirus transcription machineries respond to uncoating. *J. Virol.* (2018). doi:10.1128/JVI.00774-18
32. Makeyev, E. V. & Bamford, D. H. The polymerase subunit of a dsRNA virus plays a central role in the regulation of viral RNA metabolism. *EMBO J.* **19**, 6275–6284 (2000).
33. Patton, J. T., Jones, M. T., Kalbach, A. N., He, Y. W. & Xiaobo, J. Rotavirus RNA polymerase requires the core shell protein to synthesize the double-stranded RNA genome. *J. Virol.* **71**, 9618–9626 (1997).
34. Tortorici, M. A., Broering, T. J., Nibert, M. L. & Patton, J. T. Template recognition and formation of initiation complexes by the replicase of a segmented double-stranded RNA virus. *J. Biol. Chem.* **278**, 32673–32682 (2003).

35. Petrov, A. S. & Harvey, S. C. Packaging double-helical DNA into viral capsids: structures, forces, and energetics. *Biophys. J.* **95**, 497–502 (2008).

Figure Legends

Figure 1 | Structure of $\phi 6$ nucleocapsid and dsRNA genome. **a**, Structure of the $\phi 6$ nucleocapsid seen along an icosahedral two-fold symmetry axis (ellipse). A three-fold axis (black line) is denoted with triangle. The positions of four P4 packaging NTPase (gray) are indicated. Different subunits of P8 that build the outer shell are colored in yellow, green, gold and brown. Different subunits of P1 that build the inner protein shell are colored in blue and red. Scale bar, 200 Å. **b**, A cut open view of the structure in the same orientation as in **a** showing the dsRNA density (purple) proximal to the P1 shell reconstructed without symmetry. Areas where the RNA transitions from the first layer to the second are indicated with triangles. The left inset shows a model of dsRNA (purple) built into the density (transparent surface) showing the major (filled triangles) and minor (open triangles) grooves. The right inset shows and area with RNA transitioning from the first layer (purple) to the second layer (cyan). **c**, The same dsRNA density as in **b** is shown in four different views (indicated by a rotation around an axis by the angle given). A cage with D3 symmetry (gray) is shown as a reference. **d**, Histogram showing the number of base pairs at different distances from the virion center. The RNA is organised in five layers (1–5) numbered consecutively from outside to inside. **e**, A slab cutting through the full genome model (ribbons) showing parts for all the five layers (colored as in **d**). **f**, Complete models are shown as ribbons for the five layers (colored as in **d** and **e**). Mean values for α (arc), the angle between a segment of RNA (double dashed line) and the spool long axis (arrow) as indicated in the schematic, are given.

Figure 2 | Organization of the dsRNA genome. **a**, Local density is plotted as a histogram separately for the five layers. The mean and standard deviation of a fitted Gaussian function is given for each layer. **b**, The genome model is shown along the pseudo three-fold axis and colored based on local density. The front half is removed to show the middle part of the spool. **c**, The same model as in **b** is shown rotated as indicated and a slab of RNA is shown. The insets show two areas with high density. **d**, Polygonality index histogram is shown for the five layers. **e**, The genome model is shown along the pseudo three-fold axis with cubic and hexagonal regions colored. **f**, The same model as in **e** is shown rotated as indicated and a slab of RNA is shown. The insets show the same areas as in **c** and reveal hexagonal (top) and cubic (below) packing. **g**, Curvature value histogram for the five layers. The mean and standard deviation of a fitted Gaussian function is given for each layer. **h**, A slab of the model is shown to highlight areas of high curvature at the top of the spool. The inset shows a nearly straight area of the genome in the first (1) and the second layer (2). **i**, A slab of the model in **h** is shown rotated as indicated to show the nearly straight stands in the middle of the spool.

Figure 3 | Organizational heterogeneity in the genome. **a**, Organization of the genome with pseudo D3 symmetry (denoted as $pD3'$, see Extended Data Fig 1) is

shown along the pseudo three-fold axis of symmetry. **b**, Organization of the genome with pseudo C2 symmetry ($pC2$) is shown in the same orientation as in **a**. **c–d**, The organizations shown in **a** and **b** are shown rotated by 90 degrees as indicated. **e**, Three sub-organizations of $pD3'$ shown in **a** and **c** ($pD3'$ -1, $pD3'$ -2, $pD3'$ -3) are rotated as indicated to reveal their differences. **f**, Close-ups of the three sub-organizations shown in **e** are in the same order and orientation and colored as in Fig 1. In $pD3'$ -2 and $pD3'$ -3, different transitions of dsRNA from the first layer (purple) to the second layer (cyan) are indicated with arrowheads. Note that both of these transitions are absent in $pD3'$ -1.

Figure 4 | Putative interactions between RNA and P1 shell. **a**, Density (from the D3 map), atomic models corresponding to the P1 shell (in $pD3'$ -1 organization, blue backbone, $P1_A$) and the RNA genome (dsRNA) are shown. P1 helix 205–217 which is often in close proximity to the RNA is indicated with an arrow head. **b**, A close-up between two asymmetric units showing two $P1_A$ chains (blue and teal). Helix 205–217 is indicated with an arrowhead. **c**, A close-up of different types of putative interactions in two $P1_A$ subunits (teal, N570; blue, K208 and K217 from helix 205–217). **d**, The two lysines of helix 205–217 (K208 and K215) are shown from an asymmetric unit where the helix in $P1_B$ subunit lies on top of the RNA orthogonal to it. A methionine (M209) pointing away from the RNA is labelled. **e**, A close up of $P1_B$ helix 205–217 from an asymmetric unit where the helix is parallel to two strands of RNA and wedges between them. **f**, A close-up of $P1_B$ helix 205–217 from an asymmetric unit where the helix is at considerable distance from the RNA.

Methods

Cryo-EM sample preparation. Bacteriophage $\phi 6$ was grown on its host *Pseudomonas syringae* pv. *phaseolicola* HB10Y³⁶ and purified in the presence of 1 mM $MgCl_2$, 0.1 mM $CaCl_2$ as described previously³⁷. Nucleocapsids were produced by Triton X-114 extraction and purified as described earlier¹⁸. A 3- μ l aliquot of sample, diluted in buffer (20 mM KPO_4 , pH 7.2, 1 mM $MgCl_2$, 0.1 mM $CaCl_2$, 150 mM NaCl) to concentration of 3 mg ml^{-1} , was applied to a glow-discharged grid (C-flat; Protochips, Raleigh, NC) and vitrified by plunge-freezing into liquid ethane using a vitrification apparatus (Vitrobot; Thermo Fisher).

Data acquisition. Data were acquired over a single four-day session using a 300-kV transmission electron microscope (Titan Krios; Thermo Fisher) equipped with a direct electron detector (Falcon II, Thermo Fisher) at eBIC, Diamond Light Source, UK. Movies (33 frames, each frame 0.0625 s) were collected at dose rate of about 32 e^- per pixel per s at calibrated magnification of 98,592 \times resulting in a total dose of 33 e^- per \AA^2 and pixel size of 1.42 \AA . Data acquisition statistics are summarized in **Extended Data Table 1**.

Data processing. Movie frames were aligned to account for drift³⁸ and contrast transfer function (CTF) parameters were estimated³⁹. A total of 4,414 movies, showing minimal drift and astigmatism were used to pick ~86,000 particles. Particles

were extracted for 2D reference free classification in Relion 1.4⁴⁰. Particles from classes showing a packaged genome and complete P1 and P8 layers were selected for 3D classification using a previously published NC structure (EMD-1206) as an initial model. A subset of ~55,000 particles extracted from movies was refined using standard refinement and particle polishing protocols implemented in Relion 2.0.3 and by applying icosahedral symmetry (**Extended Data Figure 1; Extended Data Table 2**).

To reconstruct the genome without icosahedral symmetry, the source code of Relion 2.0.3 was modified to extend the prior information used in each iteration from one orientation to the 60 icosahedrally related ones. After subtracting the contribution of the capsid using *relion_project*⁴¹, 3D classification with one class and with restricted search ranges around each of the 60 prior orientations was performed relaxing the symmetry from I1 to C1 (**Extended Data Figure 1**). The resulting map showed clear density for the outer dsRNA layer but not for the other layers suggesting that the layers might be disordered relative to each other. To improve the density of the outer layer, the classification was rerun using a mask to exclude the contribution of the inner layers. To discern between the different genome conformations, localized reconstruction²⁰ was performed on the area where the density was poorest leading to a pseudo-D3 organisation (~57% of particles) and pseudo-C2 organisation (~43% of particles). Whereas the latter class was mostly well resolved, the former class presented several density ambiguities indicating a possible overlap between multiple sub-conformations with even more subtle differences. To distinguish these sub-conformations, localized reconstruction was employed again on the same area of poorly resolved density leading to multiple well resolved classes, albeit at lower resolutions due to the decreased number of particles.

To obtain the structure of the second layer without the bias introduced by the better resolved capsid and the first layer, the density of the capsid and of the first layer were subtracted from the original images. Again, the inner layers were masked out, however, this time a local search where the angles were allowed to change ± 3 degrees was performed to account for the small deviations from the orientation of the first layer. The same procedure was applied to subsequently determine the structures of the third, fourth and fifth layers. No symmetry was applied on these layers.

Model building. A previous model of the nucleocapsid asymmetric unit containing proteins P1_A, P1_B, the C-terminus of P4 and ten chains of P8 was fitted as a rigid body in the nucleocapsid density in UCSF Chimera⁴² and the model was refined in Refmac5⁴³. To build a model of the dsRNA, 30-mers of canonical A-form dsRNA were fitted in Coot⁴⁴ as rigid bodies to serve as starting points. As the sequence of the RNA could not be assigned, the model was built using A–U base pairs. Using custom functionalities of Rosetta (available upon request from the authors)⁴⁵, the 30-mers were extended in both directions. For the strands crossing between layers, the map of the layer showing the best resolved density was used for each extension and the map of the other layer was used as validation.

Analysis of packing parameters. The mean density of dsRNA was calculated within a sphere (radius of 220 Å), after subtracting the calculated volume corresponding to 10 RdRPs (average protein density 0.81 Da/Å³), and using the total length of the genome (13,385 bp) and the average molecular weight of 682 Da

per base pair. Custom scripts were written to analyse different packing parameters from the model of the genome. In all subsequent calculations, the position of each base pair was estimated as the average across 10 neighbouring base pairs (11 base pairs in total corresponding to one full turn). The RNA packing density was calculated using all dsRNA atoms within 40 Å distance from each base pair position. For the first layer, the volume corresponding to the P1 shell was discarded by using a sphere cap with a height of 11.5 Å (the radius of A-form dsRNA). To determine polygonality, hexagonality, and cubicity for each base pair position, a plane containing the corresponding position and perpendicular to the direction of the corresponding strand was determined. The base pairs of nearby strands (closer than 50 Å) that were closest to the position of interest and closer than 3.4 Å (helix rise of A-form dsRNA) from the plane were denoted as neighbours to the base pair in question. The number of neighbours was limited to 8 with maximum 3 in adjacent layers and 2 in the same layer. The polygonality index⁴⁶, where n is the number of neighbours and a_i are the angles between consecutive neighbours, was calculated:

$$PI = \frac{1}{\frac{\sum_{i=1}^n \left| \frac{2\pi}{n} - a_i \right|}{n} + 1}$$

The neighbours that decreased the polygonality index were considered false positives and thus excluded from the calculation. Hexagonality index (HI) and cubicity index (CI) were calculated using only the 4 closest neighbours and their angular deviations from $\pi/3$ and $\pi/4$, respectively. The angle between the segments $[k+n, k]$ and $[k-n, k]$ was also determined and denoted as curvature for $n=15$ (ref 47).

References

36. Vidaver, A. K., Koski, R. K. & Van Etten, J. L. Bacteriophage phi6: a Lipid-Containing Virus of *Pseudomonas phaseolicola*. *J. Virol.* **11**, 799–805 (1973).
37. Bamford, D. H., Ojala, P. M., Frilander, M., Walin, L. & Bamford, J. K. H. [25] Isolation, purification, and function of assembly intermediates and subviral particles of bacteriophages PRD1 and $\sigma 6$. in *Methods in Molecular Genetics* (ed. Adolph, K. W.) **6**, 455–474 (Academic Press, 1995).
38. Li, X. *et al.* Electron counting and beam-induced motion correction enable near-atomic-resolution single-particle cryo-EM. *Nat. Methods* **10**, 584–590 (2013).
39. Mindell, J. A. & Grigorieff, N. Accurate determination of local defocus and specimen tilt in electron microscopy. *J. Struct. Biol.* **142**, 334–347 (2003).
40. Scheres, S. H. W. RELION: implementation of a Bayesian approach to cryo-EM structure determination. *J. Struct. Biol.* **180**, 519–530 (2012).
41. Bai, X.-C., Rajendra, E., Yang, G., Shi, Y. & Scheres, S. H. W. Sampling the conformational space of the catalytic subunit of human γ -secretase. *Elife* **4**, (2015).
42. Goddard, T. D., Huang, C. C. & Ferrin, T. E. Visualizing density maps with UCSF Chimera. *J. Struct. Biol.* **157**, 281–287 (2007).
43. Nicholls, R. A., Long, F. & Murshudov, G. N. Low-resolution refinement tools in REFMAC5. *Acta Crystallogr. D Biol. Crystallogr.* **68**, 404–417 (2012).
44. Emsley, P. & Cowtan, K. Coot: model-building tools for molecular graphics. *Acta Crystallogr. D Biol. Crystallogr.* **60**, 2126–2132 (2004).

45. DiMaio, F. *et al.* Atomic-accuracy models from 4.5-Å cryo-electron microscopy data with density-guided iterative local refinement. *Nat. Methods* **12**, 361–365 (2015).
46. da Fontoura Costa, L., Rocha, F. & Araújo de Lima, S. M. Characterizing polygonality in biological structures. *Phys. Rev. E Stat. Nonlin. Soft Matter Phys.* **73**, 011913 (2006).
47. Goodsell, D. S. & Dickerson, R. E. Bending and curvature calculations in B-DNA. *Nucleic Acids Res.* **22**, 5497–5503 (1994).

Data availability

Density maps and the model that support the findings of this study have been deposited in the Electron Microscopy Data Bank and in the Protein Data Bank with the accession codes EMD-0299 and PDB:6HY0 (nucleocapsid, icosahedral symmetry), EMD-0300 (nucleocapsid, D3 symmetry), EMD-0301 (genome first layer organization *pD3*), EMD-0302 (genome first layer organization *pD3'*), EMD-0303 (genome first layer organization *pC2*), EMD-0304 (genome first layer sub-organization *pD3'-1*), EMD-0305 (genome first layer sub-organization *pD3'-2*), and EMD-0306 (genome first layer sub-organization *pD3'-3*). Maps from the layer-by-layer genome reconstruction have been submitted with the accession codes EMD-0294 (genome second layer), EMD-0295 (genome third layer), and EMD-0296 (genome fourth and fifth layers).

Code availability

Custom software code used in this study is available from the authors upon request and from <https://github.com/OPIC-Oxford>.

Extended Data Legends

Extended Data Figure 1 | Asymmetric reconstruction of the $\phi 6$ genome. **a**, The icosahedral symmetry (I1) in the $\phi 6$ nucleocapsid reconstruction, calculated from the original cryo-EM single particles (particle images), was relaxed to allow asymmetric reconstruction. The images, where the protein shells had been subtracted (genome-only particle images), were used to calculate a D3 genome reconstruction in addition to asymmetric reconstructions that had either pseudo D3 (*pD3*) or pseudo C2 (*pC2*) symmetry. Three sub-conformations of the *pD3'* reconstruction (*pD3'-1*, *pD3'-2*, *pD3'-3*) are shown rotated as indicated to reveal their differences in RNA organisation. The names of the reconstructions that were used to model the layers of the dsRNA genome and dsRNA–P1 interactions are in bold and are indicated with dotted lines. **b–f**, Fourier shell correlation (FSC) is plotted for the reconstructions included in further analysis, namely I1, D3, *pD3*, *pC2*, and *pD3'-1*. Volume masking (Masked) was used to focus the FSC test on the area used in further modelling and this increased the estimated resolution compared to the original unmasked reconstruction (Unmasked). Possible effects of the masking were compensated for

by noise randomization (Randomized) to create the final FSC curve (Corrected). The resolution at which the correlation drops below the FSC=0.143 threshold is indicated.

Extended Data Figure 2 | Model of the $\phi 6$ genome. The cryo-EM asymmetric reconstruction (Density) and the model built into the same density (Model) are shown for each of the genome layers. The layers are colored as in Figure 1. The density shown for layer 1 is from the $pD3'$ -1 map and the density for layers 2–4 is from the $pD3$ map.

Extended Data Figure 3 | Modes of dsRNA packing in $\phi 6$. A histogram with relative frequencies of base pairs located in hexagonal, cubic and undefined packing regions. The total number of base pairs defined for each layer is provided.

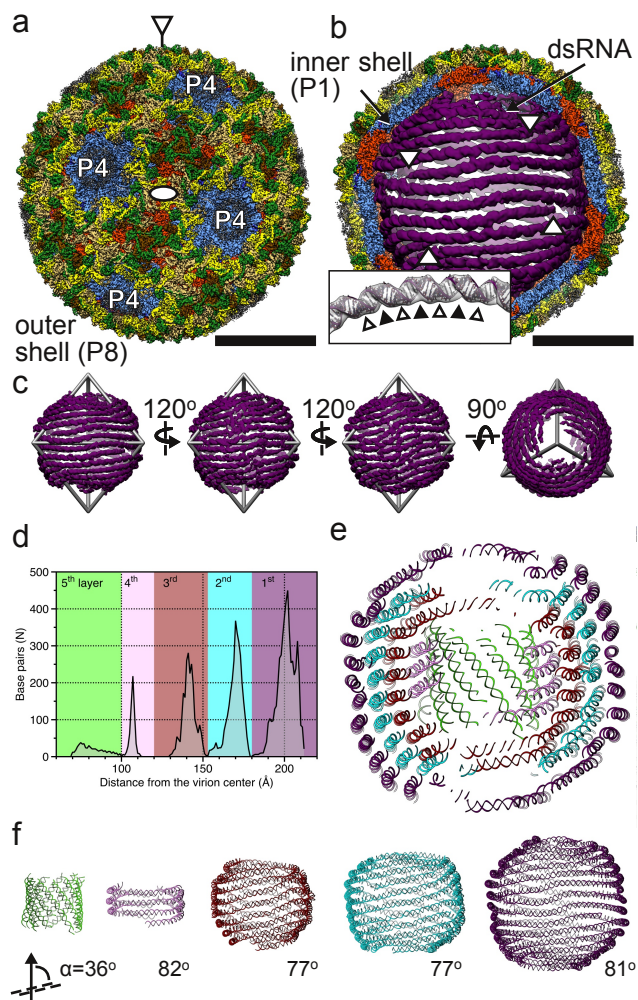
Extended Data Figure 4 | Distances between different types of P1 residues and RNA. a–b, Fractions of different P1 amino acid residue types at different distances from the RNA are shown for the $pD3$ and $pC2$ models are shown in *a* and *b*, respectively.

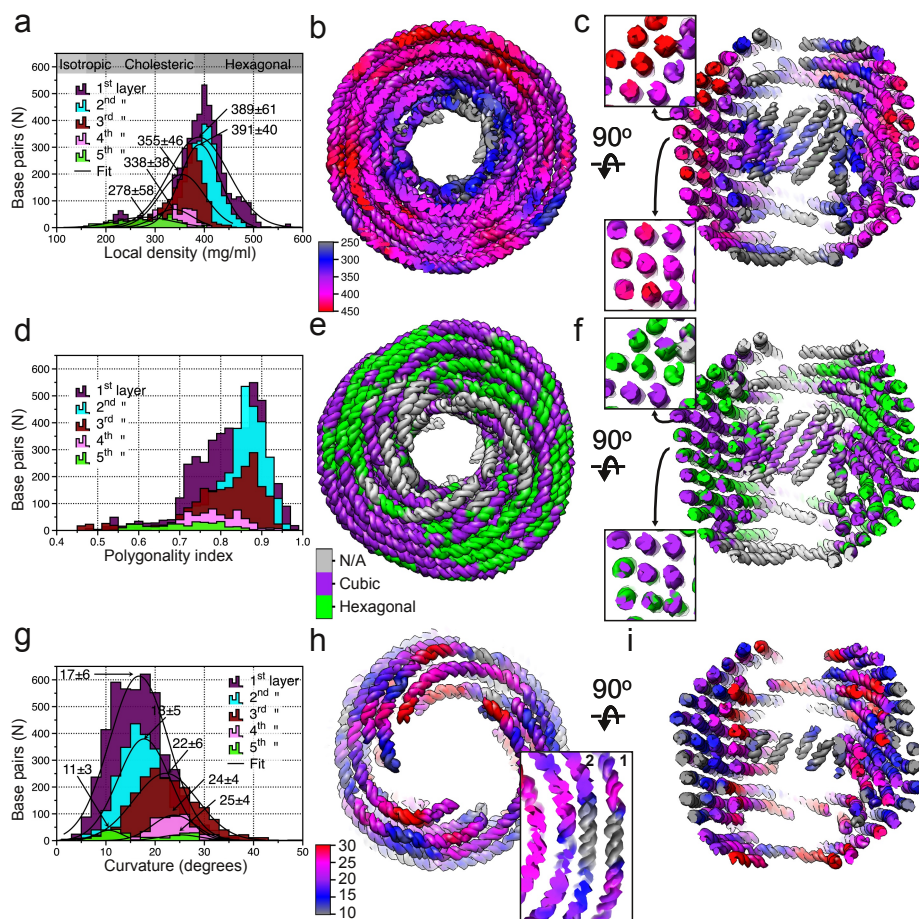
Extended Data Figure 5 | P1–RNA distances in the first genome layer with $pD3$ symmetry. The frequency of P1 residues in the $pD3$ conformation that have non-hydrogen atoms closer than 14 Å to dsRNA model non-hydrogen atoms is given in each distance bin (1–14 Å) for P1 chains A and B together (Chains A and B) and separately (Chain A and Chain B, respectively). The total number of residues with atom or atoms closer than the cutoff distance is given for each table (T). The difference in the total numbers between chains A and B is given (Comparison) as a log2 ratio (*i.e.* base-2 logarithm of the ratio of total frequencies for chains A and B). For example, value 1 means that chain A has 2 times as many included residues as chain B and value 2 means that chain A has 4 times as many included residues as chain B (negative values mean that chain B had more included residues). Those cases where an included residue was present only in one of the two chains are indicated (Only A and Only B).

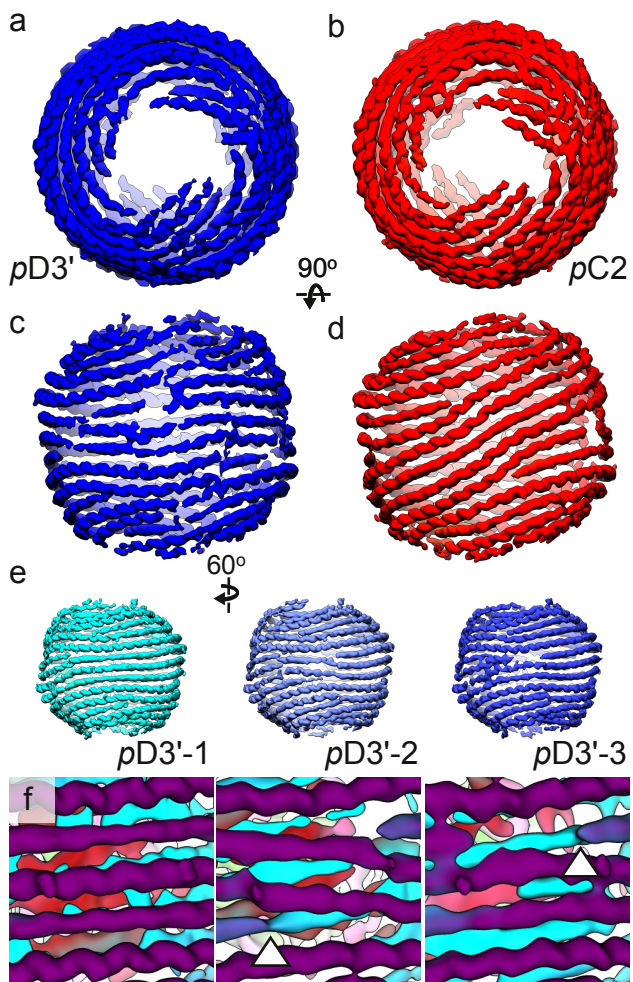
Extended Data Figure 6 | P1–RNA distances in the first genome layer with $pC2$ symmetry. The frequency of P1 residues in the $pC2$ conformation that have non-hydrogen atoms closer than 14 Å to dsRNA model non-hydrogen atoms is given in each distance bin (1–14 Å) for P1 chains A and B together (Chains A and B) and separately (Chain A and Chain B, respectively). The annotations are as in Extended Data Fig 5.

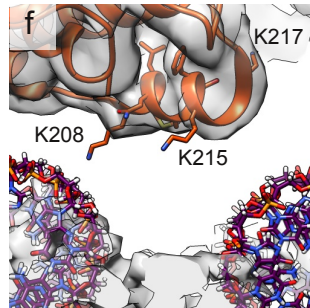
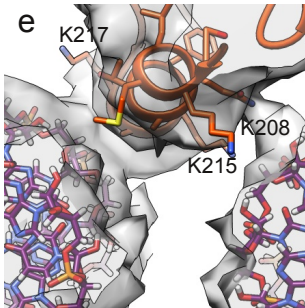
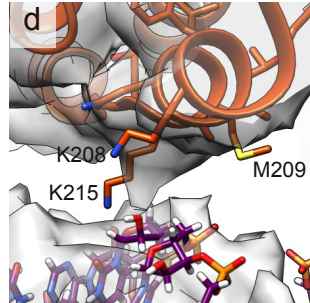
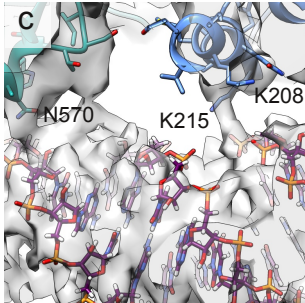
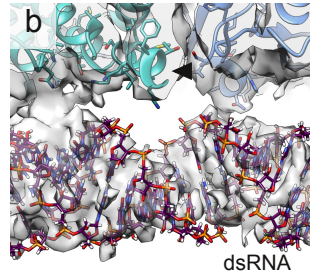
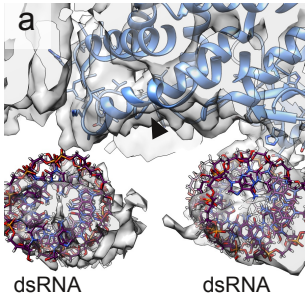
Extended Data Table 1 | Cryo-EM data collection and nucleocapsid model.

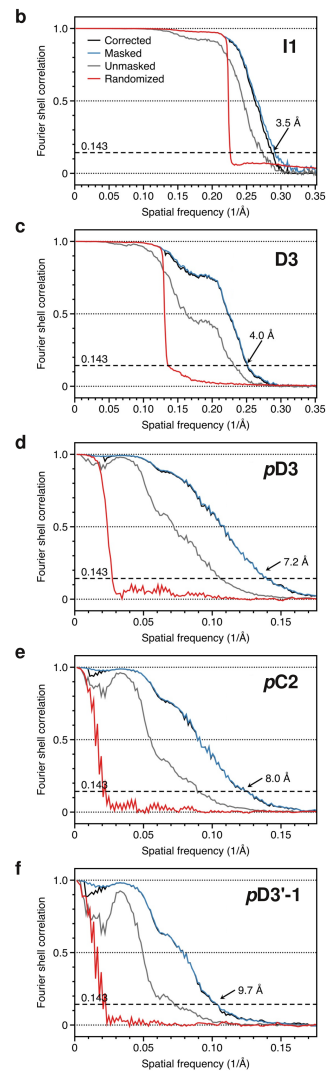
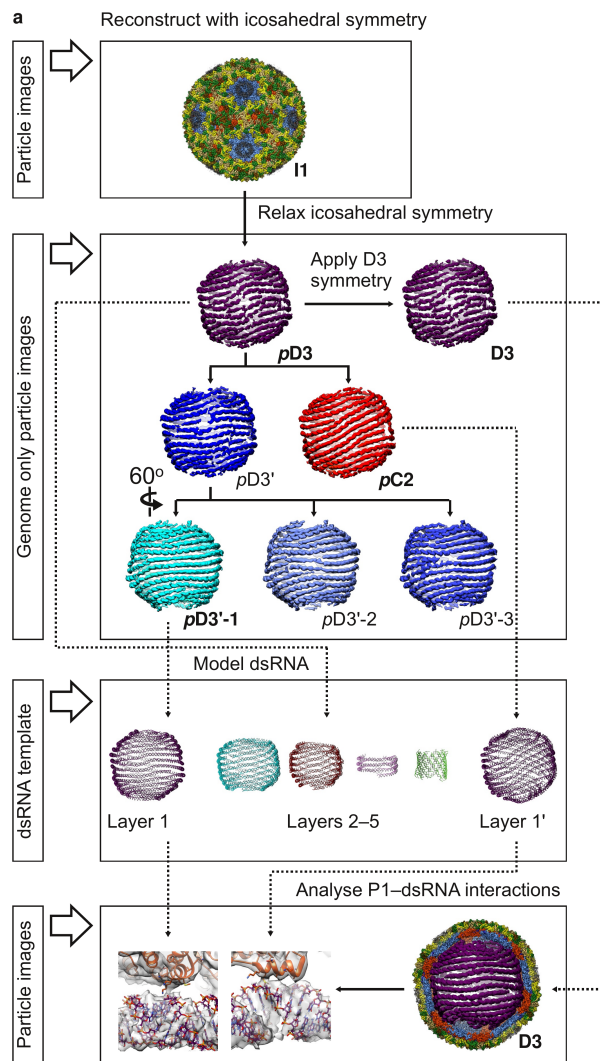
Extended Data Table 2 | Cryo-EM reconstruction parameters. * The number of the dsRNA layers is given. ** Resolution determined by Fourier shell correlation at 0.143 threshold.







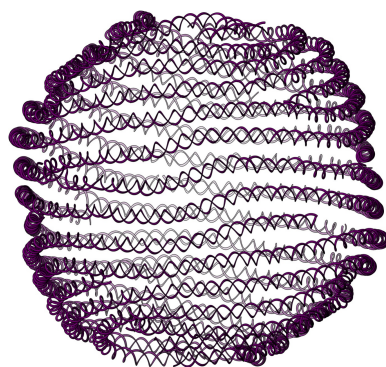
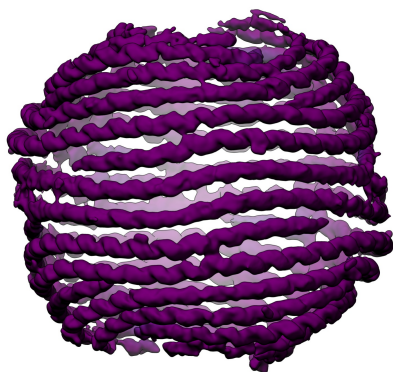




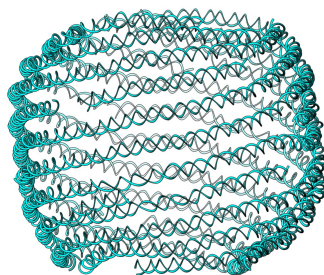
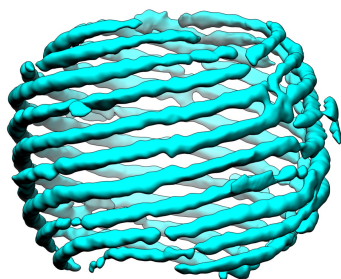
Density

Model

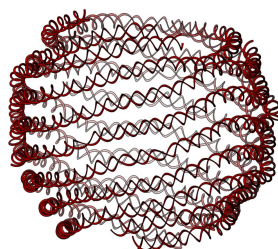
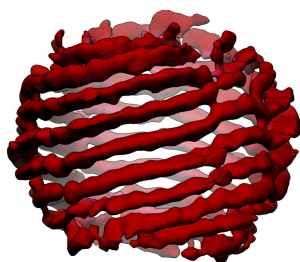
1st layer



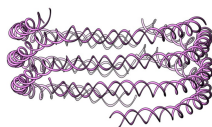
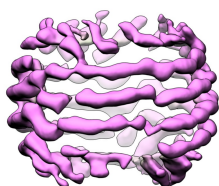
2nd layer



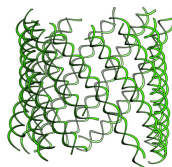
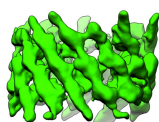
3rd layer

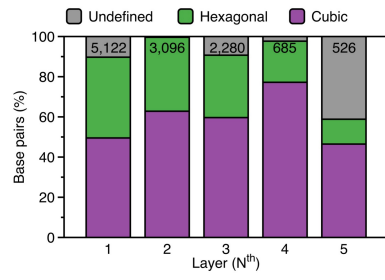


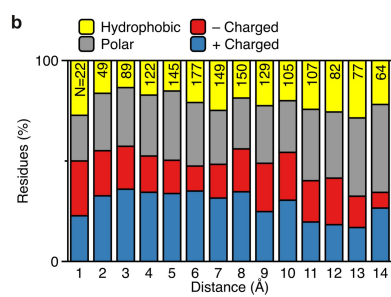
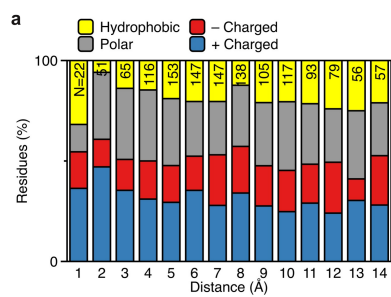
4th layer



5th layer







[illegible]

Residue	Chains A and B															Chain A	Chain B															Comparison					
	1	2	3	4	5	6	7	8	9	10	11	12	13	14	T		1	2	3	4	5	6	7	8	9	10	11	12	13	14	T						
GLN 39	0	0	0	0	0	0	0	0	0	1	1	0	0	1	3	6	0	0	0	0	0	0	0	0	0	0	0	0	0	0	0	Only A					
THR 41	0	0	0	0	0	0	0	0	0	0	0	0	0	0	1	2	0	0	0	0	0	0	0	0	0	0	0	0	0	0	0	Only A					
ARG 42	0	0	0	0	0	0	0	2	1	5	3	3	8	4	2	28	0	0	0	0	0	2	0	5	1	0	5	1	0	14	0	0	0				
LEU 52	0	0	0	0	0	0	0	0	0	0	0	0	1	0	0	0	1	0	0	0	0	0	0	0	0	0	0	0	0	0	0	Only A					
GLU 55	0	0	0	0	0	2	0	0	0	1	1	0	0	0	0	4	0	0	0	0	0	0	0	0	0	0	0	0	0	0	0	0	Only A				
GLY 59	0	0	0	0	0	0	0	0	0	1	0	0	0	0	0	1	0	0	0	0	0	0	0	0	0	0	0	0	0	0	0	0	Only A				
ASN 60	0	0	0	0	1	0	4	7	3	3	1	2	2	0	23	0	0	0	0	1	0	4	7	3	3	1	2	2	0	23	0	0	0	Only A			
ASP 62	0	0	0	0	0	0	0	2	0	0	0	0	0	0	2	0	0	0	0	0	1	0	0	0	0	0	0	0	0	0	0	0	0				
ASP 121	0	0	0	0	0	0	0	0	0	0	1	3	1	1	0	6	0	0	0	0	0	0	0	0	1	3	1	1	0	6	0	0	Only A				
LEU 161	0	0	0	0	0	1	4	4	6	5	4	0	2	1	27	0	0	0	0	0	1	4	4	6	5	4	0	2	27	0	0	0	Only A				
PRO 166	0	0	0	0	0	1	0	0	0	0	0	0	0	0	0	1	0	0	0	0	0	0	0	0	0	0	0	0	0	0	0	0	Only A				
ARG 196	0	0	0	1	0	0	0	0	0	0	0	0	0	0	0	1	0	0	1	0	0	0	0	0	0	0	0	0	0	0	0	0	Only A				
THR 200	0	0	0	0	0	2	0	0	0	0	0	0	0	1	0	3	0	0	0	0	0	0	0	0	0	0	0	0	0	0	0	0	Only A				
SER 204	0	0	0	0	0	1	0	0	0	0	0	0	0	0	0	1	0	0	0	0	0	0	0	0	0	0	0	0	0	0	0	0	Only A				
VAL 205	0	0	1	0	0	0	2	3	5	1	1	4	0	2	19	0	0	1	0	0	2	3	5	1	1	4	0	2	19	0	0	0	0	Only A			
LYS 208	0	0	1	1	1	5	6	10	4	6	14	2	5	1	56	0	0	1	0	3	0	3	2	0	3	0	1	0	13	0	0	1	0	-2			
MET 209	0	1	0	0	1	3	5	1	4	6	1	1	0	0	23	0	0	0	0	0	0	0	0	0	0	0	0	0	0	0	0	0	0	Only B			
GLN 211	0	0	0	0	0	0	1	3	2	0	0	0	0	0	7	0	0	0	0	0	1	1	2	1	0	0	0	0	5	0	0	0	0	1			
LYS 215	0	0	0	0	4	5	8	11	10	10	9	8	5	2	72	0	0	0	0	0	1	4	9	6	5	6	4	3	2	40	0	0	0	32	0		
ALA 216	1	1	1	3	4	8	15	7	7	3	3	4	3	0	60	0	1	1	1	0	3	1	1	3	1	2	0	0	14	1	0	0	2	-2			
ARG 276	0	0	0	0	0	0	0	0	0	0	3	3	5	5	3	19	0	0	0	0	0	0	0	3	3	5	5	3	19	0	0	0	0	Only A			
ASN 277	0	0	0	0	0	0	0	0	0	0	0	0	0	1	0	1	0	0	0	0	0	0	0	0	0	0	0	0	1	0	0	0	0	Only A			
THR 278	0	0	0	0	0	0	0	1	1	3	1	0	0	0	0	6	0	0	0	0	0	0	0	0	0	0	0	0	0	6	0	0	0	Only A			
ASN 279	0	0	3	6	8	7	8	10	9	8	10	9	2	2	82	0	0	3	6	7	5	8	2	5	0	2	4	1	0	43	0	0	0	1	0		
ASP 282	0	1	0	3	6	3	0	2	3	1	7	2	1	1	30	0	1	0	3	6	3	0	2	3	1	7	1	1	1	29	0	0	0	0	5		
GLN 283	0	0	0	0	1	0	0	1	1	0	0	0	0	0	3	0	0	0	0	1	0	0	1	0	0	0	0	0	3	0	0	0	0	Only A			
GLU 323	0	0	0	0	0	0	0	0	2	1	4	2	5	0	14	0	0	0	0	0	0	0	0	0	0	1	1	2	0	4	0	0	0	-1			
SER 326	0	0	0	1	0	2	1	0	0	0	0	0	0	0	6	0	0	0	0	0	0	0	0	0	0	0	0	0	0	0	0	0	0	Only B			
GLU 327	0	0	0	1	0	0	2	6	3	6	5	0	4	2	29	0	0	0	1	0	0	2	5	2	4	3	0	3	1	21	0	0	0	0	1		
VAL 328	0	0	0	0	0	0	1	1	2	0	2	1	1	2	10	0	0	0	0	0	0	0	0	0	0	0	0	0	0	0	0	0	0	Only B			
LYS 332	0	0	0	0	0	5	4	4	7	11	13	10	4	4	62	0	0	0	0	0	5	2	4	4	3	3	1	0	1	23	0	0	0	0	-1		
LEU 333	0	0	0	0	0	1	0	2	0	0	0	0	0	0	3	0	0	0	0	1	0	2	0	0	0	0	0	0	3	0	0	0	0	Only A			
PRO 335	0	1	1	0	0	8	7	2	2	2	3	0	0	0	27	0	0	0	0	0	2	1	0	0	0	0	0	0	3	0	1	1	0	0	-3		
ASN 337	0	0	0	2	2	4	4	8	5	2	1	0	2	0	30	0	0	0	0	0	2	6	4	1	1	0	1	0	15	0	0	0	0	0	0		
GLU 338	0	0	0	0	2	1	5	11	6	6	3	0	2	0	36	0	0	0	0	1	1	4	7	3	4	1	0	2	0	23	0	0	0	0	1		
GLN 365	0	0	0	0	1	0	1	4	2	4	4	7	6	2	31	0	0	0	0	1	0	1	3	2	3	3	3	4	1	21	0	0	0	0	10		
LYS 368	0	0	0	0	0	0	0	2	3	3	2	6	6	5	25	0	0	0	0	0	0	0	0	0	0	0	0	0	1	3	0	0	0	0	-3		
GLU 369	0	0	0	0	0	2	2	9	2	4	2	3	2	2	26	0	0	0	0	0	0	1	2	1	7	0	2	0	3	16	0	0	0	0	1		
ASP 395	0	0	0	0	0	0	3	1	1	1	1	0	2	2	11	0	0	0	0	0	0	2	1	1	1	1	0	2	1	9	0	0	0	0	0	2	
ALA 399	0	0	0	0	0	1	1	0	0	0	1	1	1	0	5	0	0	0	0	1	0	0	0	0	0	0	0	0	0	1	0	0	0	0	-2		
ALA 402	0	0	0	0	0	0	0	0	0	0	1	2	0	0	3	0	0	0	0	0	0	0	0	0	0	0	0	0	2	0	0	0	0	0	1		
ASN 406	0	0	0	0	0	1	10	6	7	10	10	5	5	5	54	0	0	0	0	0	0	0	1	1	2	3	3	2	15	0	0	0	0	0	0	-1	
GLU 500	0	0	0	0	0	0	0	0	0	0	0	0	0	1	0	0	0	0	0	0	0	0	0	0	0	0	0	1	0	0	0	0	0	0	Only A		
ARG 523	0	0	0	0	0	0	2	2	7	1	2	2	5	2	21	0	0	0	0	0	0	2	2	7	1	2	2	5	21	0	0	0	0	0	0	Only A	
GLU 525	0	0	0	0	1	1	2	1	1	0	2	1	2	1	10	0	0	0	0	1	1	2	1	1	0	2	1	2	10	0	0	0	0	0	0	Only A	
LYS 553	0	0	0	0	0	0	1	0	2	1	0	1	2	1	8	0	0	0	0	0	0	0	0	0	0	0	0	0	0	0	0	0	0	0	0	Only A	
GLN 556	0	0	0	0	0	1	1	0	2	5	4	4	3	2	20	0	0	0	0	0	0	1	1	0	2	1	0	3	9	0	0	0	0	0	0	0	11
SER 558	0	0	0	0	0	0	0	0	0	0	1	1	0	2	9	0	0	0	0	0	0	0	0	0	0	0	0	0	0	2	3	0	0	0	-1		
GLU 559	0	0	0	1	1	1	5	3	8	6	7	6	4	2	44	0	0	0	1	1	1	4	1	4	3	5	2	2	0	24							

	Nucleocapsid (EMD-0299) (6HY0)
Data collection and processing	
Magnification	98,592
Voltage (kV)	300
Electron exposure (e ⁻ /Å ²)	33
Defocus range (μm)	0.3–3.0
Pixel size (Å)	1.42
Initial particle images (no.)	86,114
Final particle images (no.)	55,265
Map resolution (Å)	3.5
FSC threshold	0.143
Refinement	
Initial model used (PDB code)	5MUU
Initial model resolution (Å)	4.0
FSC threshold	0.143
Model resolution (Å)	3.5
Map sharpening <i>B</i> factor (Å ²)	−240
Model composition	
Non-hydrogen atoms	23,386
Protein residues	3,051
Ligands	0
<i>B</i> factors (Å ²)	
Protein	31
Ligand	N/A
R.m.s. deviations	
Bond lengths (Å)	0.35
Bond angles (°)	0.57
Validation	
MolProbity score	1.41
Clashscore	3.51
Poor rotamers (%)	0.1
Ramachandran plot	
Favored (%)	96
Allowed (%)	4
Disallowed (%)	0

	NC (I)	NC (D3)	<i>p</i>D3 layer* 1	<i>p</i>D3 layer 2	<i>p</i>D3 layer 3	<i>p</i>D3 layers 4–5	<i>p</i>D3' layer 1	<i>p</i>C2 layer 1	<i>p</i>D3'-1 layer 1	<i>p</i>D3'-2 layer 1	<i>p</i>D3'-3 layer 1
Particles	55,265	55,265	55,265	55,265	55,265	55,265	31,372	23,893	8,610	7,015	6,648
Symmetry	I1	D3	C1	C1	C1	C1	C1	C1	C1	C1	C1
Resolution (Å)**	3.5	4.0	7.2	13.5	16.2	16.9	8.0	8.0	9.7	10.2	10.2
B-factor (Å ²)	240	220	N/A	N/A	N/A	N/A	N/A	N/A	N/A	N/A	N/A
Accession code	EMD-0299	EMD-0300	EMD-0301	EMD-0294	EMD-0295	EMD-0296	EMD-0302	EMD-0303	EMD-0304	EMD-0305	EMD-0306